ROYAL SOCIETY
OF CHEMISTRY

PAPER

CrossMark
click for updates

In situ monitoring of TiO$_2$(B)/anatase nanoparticle formation and application in Li-ion and Na-ion batteries†

M. Søndergaard,[ab] K. J. Dalgaard,[a] E. D. Bøjesen,[a] K. Wonsyld,[b] S. Dahl[b] and B. B. Iversen*[a]

Bronze phase, TiO$_2$(B), and anatase nanoparticles in various weight fractions and with different sizes have been synthesized by a very facile method and their electrochemical performances have been evaluated in Li- and Na-ion cells. The transition from a layered hydrogen-titanate precursor to TiO$_2$(B)/anatase mixtures was monitored by *in situ* powder X-ray diffraction from room temperature to 800 °C. Simple NaOH treatment of the precursor inhibited the transformation of the precursor and TiO$_2$(B) to anatase at elevated temperatures and allowed for the preparation of larger TiO$_2$(B) crystallites with extra high thermal stability.

1. Introduction

TiO$_2$ is known to be a very versatile material that has useful properties for a wide range of applications *e.g.* solar cells, photocatalysis, and photo-induced water-splitting.[1] Furthermore, in the search for new anode materials for highly successful Li-ion batteries and emerging Na-ion batteries, there are now numerous reports on the promising electrochemical performance of TiO$_2$ in Li- and Na-ion half-cells.[2–11] For Li-ion battery anodes, competing with commercial graphite and Li$_4$Ti$_5$O$_{12}$ materials in terms of cost, safety and electrochemical performance is challenging. However, the low cost, high abundance, low toxicity and relatively high theoretical capacity of TiO$_2$ (335 mA h g^{-1}, compared with 372 mA h g^{-1} for graphite and 175 mA h g^{-1} for Li$_4$Ti$_5$O$_{12}$) make it a potential candidate. Among the different TiO$_2$ polymorphs, TiO$_2$(B) (space group *C2/m*) has been reported in several studies to have superior electrochemical performance in Li-ion cells, especially regarding capacity, rate-ability and lowered voltage compared with rutile and anatase.[12–15] The drawbacks of the TiO$_2$(B) polymorph are low natural abundance and syntheses involving several steps. Most reports employ a synthesis method similar to the one devised by Marchand *et al.*[16] involving proton-exchange of Na- or K-titanates and subsequent heating. However, in recent studies several other synthesis routes have been employed *e.g.* TiCl$_4$ and ionic liquids,[17] tetrabutyltitanate, polyethylene

pyrrole and acetic acid,[14] TiCl$_3$ and ethyleneglycol[18] or Ti metal dissolved in H$_2$O$_2$ and NH$_4$OH with the addition of glycolic acid and H$_2$SO$_4$.[19] Different choices of precursors and treatments lead to mixtures of TiO$_2$(B) and anatase nanoparticles or TiO$_2$(B) with different sizes and/or different morphologies, *e.g.* nanosheets,[18] nanowires[20] and nanotubes.[21] These differences all affect the electrochemical performance of the material. In the present study, a synthesis method employing titanium isopropoxide, ethyleneglycol and NH$_4$OH as precursors to produce TiO$_2$(B) is thoroughly investigated. NaOH is utilized to inhibit the transformation from TiO$_2$(B) to anatase at elevated temperatures. Additionally, the transformation from the precursor to the TiO$_2$(B)/anatase mixtures is monitored by *in situ* high-temperature (HT) powder X-ray diffraction (PXRD). Finally, the electrochemical performance of the products in Li-ion and Na-ion half-cells is investigated and related to the TiO$_2$(B)/anatase ratios and crystallite sizes.

2. Experimental details

Synthesis

TiO$_2$(B)/anatase nanoparticles were prepared by a method inspired by earlier reports.[12,18,22] Briefly, titanium(ɪᴠ)isopropoxide, Ti(OC$_3$H$_7$)$_4$ (TTIP), was mixed with ethyleneglycol (EG) in different volume ratios and with the addition of 25% NH$_3$ in water (NH$_4$OH) and heated in Teflon lined autoclaves or oil baths at 150 °C for four to 72 hours. The volume ratio TTIP : EG : NH$_4$OH 8 : 24 : 1 was selected for a temperature study and autoclave synthesis was done at temperatures of 125, 150, 175, 200, and 225 °C, for 72 hours. No solids were obtained by treatment at 100 °C while 275 °C for four hours yielded rutile in a black oil suspension. Finally, the sample autoclaved at 225 °C was subsequently heated in air for two hours at

[a]*Center for Materials Crystallography, Department of Chemistry and iNANO, Aarhus University, DK-8000 Aarhus C, Denmark. E-mail: bo@chem.au.dk*

[b]*Haldor Topsøe A/S, Nymøllevej 55, 2800 Kgs. Lyngby, Denmark*

† Electronic supplementary information (ESI) available: Additional powder X-ray diffractograms, TEM-images, photograph of samples, and results of thermal analysis. See DOI: 10.1039/c5ta04110d

This journal is © The Royal Society of Chemistry 2015

J. Mater. Chem. A, 2015, **3**, 18667–18674 | 18667

temperatures between 300 and 600 °C with and without NaOH treatment. This treatment typically involved adding 20 mL deionized water to 1 g of dried autoclaved sample and 1 mL 2 mol L^{-1} NaOH followed by magnetic stirring for 20 min before heating. The following nomenclature will be used for the samples *e.g.* "T225-400NaOH" for a sample prepared by autoclaving at 225 °C and then dried and calcined at 400 °C in air for two hours with added NaOH.

Structural and microstructural analysis

Room temperature (PXRD) patterns were collected on a Rigaku SmartLab diffractometer configured with a rotating anode CuK$_{\alpha}$ source, parallel beam optics and a D/tex Ultra 1D detector. The TiO$_2$(B)/anatase ratio, the lattice parameters and the average crystallite sizes along the crystallographic *a*-, *b*- and *c*-directions were determined by Rietveld refinement utilizing the Fullprof software suite[23] in a similar fashion as described in detail by Lock *et al.*[24] This involved employing a general phenomenological model, which contained an anisotropic size model function, and the Scherrer formula with the assumption that the size broadening can be written as a linear combination of spherical harmonics[25] as proposed by Popa.[26] In all refinements, potential profile broadening due to microstrain and defects was ignored; however the instrumental contribution to the profile broadening was accounted for by refinements of a LaB$_6$ standard under the same experimental conditions. Transmission Electron Microscopy (TEM) images were collected using a Phillips CM20 200 kV TEM. The Brunauer–Emmett–Teller (BET) specific surface area was determined by using nitrogen adsorption–desorption isotherm measurements at 77 K on a Quantachrome NOVA2200e.

In situ high temperature PXRD measurements

For the *in situ* high temperature PXRD investigations, dried precursor powders were placed in an Anton Paar dome hot stage (DHS1100). A thin quartz disk was used to protect the heating stage. The samples were heated in air from room temperature to 800 °C with a heating rate of 1 °C min^{-1}. During heating, PXRD patterns were collected using a Rigaku SmartLab diffractometer with specifications as mentioned in the above section. Diffraction patterns were collected over a 2θ range from 12° to 52° at a rate of 7 min and 20 s per scan. Thus, each diffractogram experienced a ~7 °C difference in temperature, between the beginning and end of each scan. All HT-PXRD patterns are shown with the starting temperature of the scan.

Thermal analysis

The thermal behavior of the precursor was studied by simultaneous thermogravimetric (TG) and Differential Thermal Analysis (DTA) using a Netzsch STA 449 C in an Ar/O$_2$ atmosphere. The dried precursor powders were heated from room temperature to 800 °C at a heating rate of 10 °C min^{-1}, and a continuous Ar/O$_2$ flow was applied with flow rates of 30 and 20 mL min^{-1} for Ar and O$_2$, respectively. Ar was used as a protective gas at a flow rate of 40 mL min^{-1}.

Electrochemical properties

For electrochemical measurements, CR2032 type coin-cells were assembled with either Li or Na metal foil as counter and reference electrodes. The working electrode was prepared from TiO$_2$ powder as the active material, acetylene black as the conductor, and polyvinylidene difluoride (PVDF) as the binder in the weight ratio of 76 : 12 : 12 and coated onto Al-foil using a coating bar. The typical thickness of a dry electrode was ~30 μm or ~2 mg cm^{-2}. The working electrodes were compressed with 80 kN cm^{-2}. The electrodes were separated by membranes consisting of either two pieces of 25 μm thick porous polypropylene membranes (Li-cells) or a glass fiber membrane (Na-cells). The electrolyte solution for Li-cells was composed of 1 mol L^{-1} LiPF$_6$ in ethylene carbonate (EC) and dimethyl carbonate (DMC) in the ratio of 1 : 1 by volume. The electrolyte solution for Na-cells was composed of 1 mol L^{-1} NaClO$_4$ in polycarbonate (PC) and fluoroethylene carbonate (FEC) in the ratio of 98 : 2 by volume. The cells were assembled in a glovebox with water and oxygen levels at ~1 ppm. After assembly, the cells were discharged and charged with a constant current at different C-rates (1C = 335 mA h g^{-1}) between 1.0 V and 3.0 V (Li-ion cells) and 0.1 V and 3.0 V (Na-ion cells). At least two (generally three) cells were produced for each material to ensure reproducible results.

3. Results

Synthesis and structure

Initially, the effect of changing the EG : TTIP ratio was investigated at a synthesis temperature of 150 °C and it was found that ratios 15 : 1, 5 : 1 and 3 : 1 yielded similar results, while a ratio of 1 : 1 led to deviations (see Fig. 1 for diffractograms of the as-prepared samples). The EG : TTIP ratio of 3 : 1 and an autoclaving time of 72 hours were selected for the temperature studies (PXRD of T125–T225 in Fig. 1). The diffractograms of samples T125–T225 probably represented a layered titanate structure, and similar structures have been observed in previous reports.[12,18] Several peaks were in common with those of the TiO$_2$(B) phase, but the patterns could not be refined to the TiO$_2$(B) phase. The diffractograms in Fig. 1 have been cut-off at 2θ = 10° due to a very high intensity peak usually at 7–9° (see the ESI† for full PXRD patterns). This low-angle reflection shifted with temperature from 2θ = 8.20° for T175, at 8.43° for T200 and at 8.58° for T225. The 2θ value of 8.20° corresponded to a *d*-spacing of 10.8 Å. Xiang *et al.*[18] and Liu *et al.*[12] observed similar peaks when using comparable synthesis methods. However, while only TiCl$_3$ and EG were used by Xiang *et al.*,[18] it was necessary to add 25% NH$_4$OH in the present synthesis to prevent the formation of a crystalline metal–organic compound which otherwise formed (see ESI†). In order to obtain a size estimate of the crystallites in the as-prepared samples, without knowing the structure, a single peak fit of the intense peak near 25° was performed in *WinPLOTR* under the assumption that the peak was indeed one single peak and not multiple overlapping peaks. The obtained sizes are presented in Table 1 and can be seen to increase with temperature from 3.0 nm for T125 to
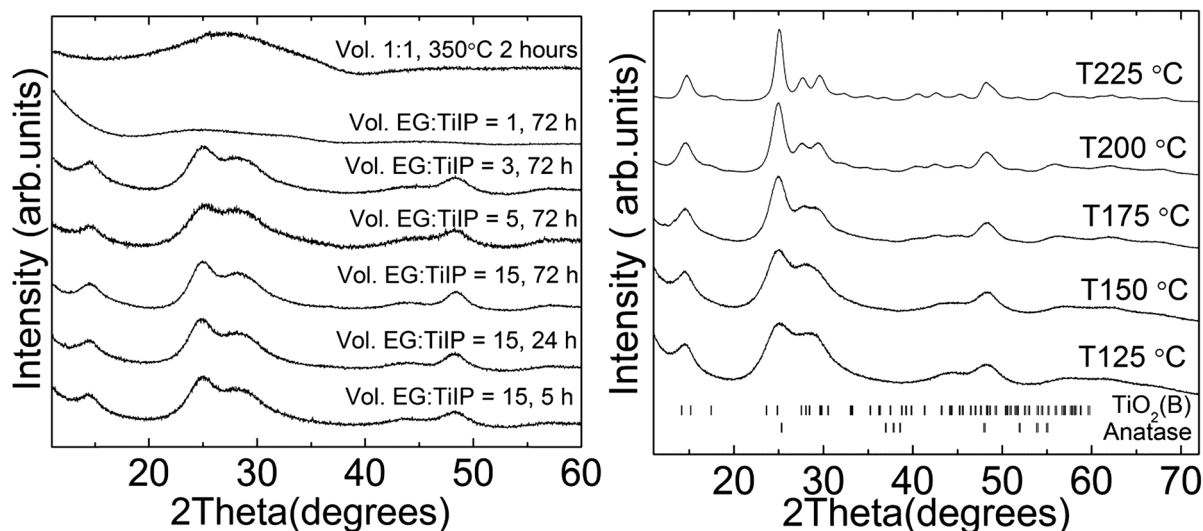
18668 | *J. Mater. Chem. A*, 2015, **3**, 18667–18674

This journal is © The Royal Society of Chemistry 2015

Fig. 1 Left: PXRD patterns of products synthesized from mixtures with different EG : TiIP ratios in an autoclave or oil bath at 150 °C. Right: temperature series with the EG : TiIP ratio 3 : 1, autoclaved for 72 h.

8.0 nm for T225. It should be noted that these sizes were not corrected for instrumental broadening and thus the actual sizes are larger than stated here. The trend will, however, still be valid. Furthermore, the reflections shifted to higher angles with temperature, corresponding to decreased unit cell parameters and decreased lattice strain.

The T225 sample was selected for heating in air at various temperatures, with or without the addition of NaOH. Collected PXRD patterns are presented in Fig. 2 along with an example of a Rietveld refinement of the T225–400 sample. The results from the Rietveld refinements of the products are presented in Table 2. The refined anatase weight fraction of the crystalline part of the samples increased with calcination temperature from 14 wt% for T225–300 to 89 wt% for T225–400; however, the NaOH-treated samples showed a considerably smaller amount of the anatase phase. Even when the temperature was increased to 600 °C, TiO_2(B) remained in the main phase with 75 wt% (see Fig. 3). It should be noted that the weight fractions of the phases are relative to each other and do not represent absolute weight fractions. There may still be amorphous material left in the sample even after the heat-treatments. It may be that sodiation of the less dense TiO_2(B) stabilizes the structure and prevents it from transforming into the more compact anatase form. The sizes of the crystallites of both phases were generally seen to increase with temperature starting from *ca.* 2 nm for TiO_2(B) and 4 nm for anatase at 300 °C and increased up to 6 nm for

TiO_2(B) and 19 nm for anatase at 600 °C. Furthermore, the anisotropy of the crystallites of both TiO_2(B) and anatase decreased with increasing temperature. Several of the refined unit cell parameters deviated significantly (>2%) from the values found in the inorganic crystal structure database (ICSD), anatase $a = 3.7842$ Å and $c = 9.5146$ Å, and TiO_2(B) $a = 12.1787$ Å, $b = 3.7412$ Å and $c = 6.5249$ Å. For anatase, generally the *a*-values were found to be larger, while the *c*-values were smaller. For the bronze phase, all lattice parameters were generally larger than the ICSD-values. These deviations were most significant for the smallest crystals and they concurred with the considerable macrostrain[27] and thus altered unit cell parameters that are often seen for nanosized crystallites. For anatase particles, negative macrostrain (corresponding to compression) of up to 1% of the *c*-values has been reported.[28] Several mechanisms cause strain in anatase and different combinations can yield different outcomes. Firstly, an increased curvature of the surface for small crystallites generates a positive pressure and thus negative macrostrain.[28] Secondly, surface defect dipoles generated from Ti-atoms coordinated to surrounding water molecules repel each other and cause a negative pressure.[29] Finally, Ti^{4+} vacancies in the structure lead to expansion in the *a*–*b*-plane and shortening of *c*.[28] With these effects in mind the positive and negative macrostrains along the *a*- and *c*-axis, respectively, suggests the presence of Ti^{4+} vacancies, which is common for nanosized TiO_2.[30] Similar mechanisms causing

Table 1 Mass loss according to TG and crystallite sizes estimated from single peak fits

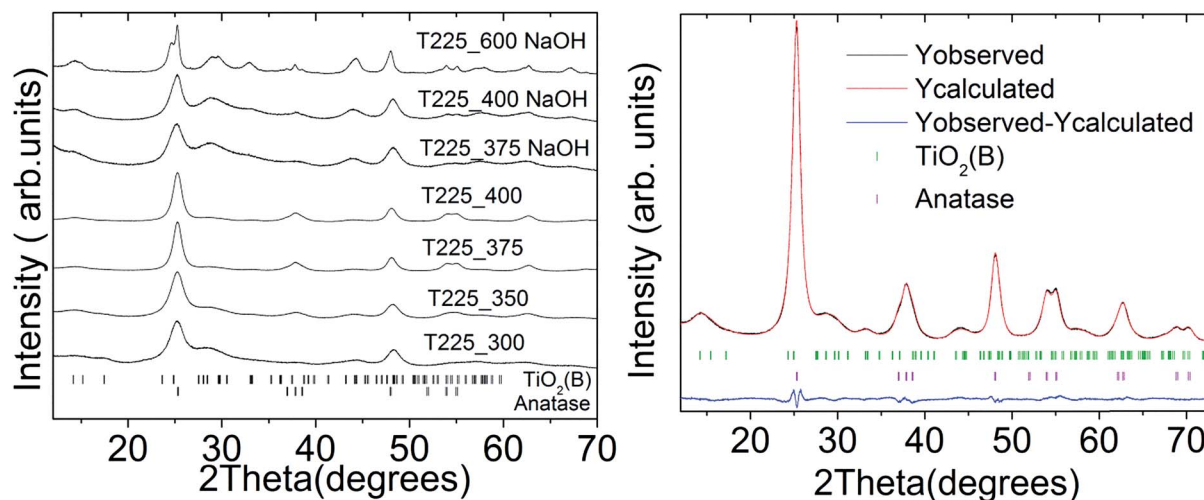| Sample	T125	T150	T175	T200	T225
TG mass loss w%	39.7 (5)	36.7 (5)	37.1 (5)	35.4 (5)	36.6 (5)
Crystallite size (nm)	3.0 (2)	3.2 (2)	3.9 (3)	5.2 (4)	8.0 (6)
FWHM (degree)	2.7 (2)	2.6 (2)	2.07 (4)	1.56 (1)	1.011 (3)
Position, 2θ (degree)	24.82 (3)	24.81 (2)	24.919 (9)	24.936 (4)	25.063 (1)

Fig. 2 Left: diffractograms of the T225 °C sample calcined for two hours at different temperatures with and without NaOH addition. Right: example of Rietveld refinement of the T225–400 °C sample.

strain and altered unit cell parameters are probable for $TiO_2(B)$. The larger deviance of the $TiO_2(B)$ lattice parameters compared with the ICSD-values could be due to the even smaller crystallite sizes. Selected TEM images of the as-prepared T225 and heated samples are shown in Fig. 4. Minute crystallites of <5 nm were readily observed. The apparent growth of crystallites upon heat treatment observed in the micrographs was in agreement with the results from PXRD (see the ESI† for more TEM images). However, due to the heavy agglomeration and lack of well-defined boundaries, a more accurate size-determination from the TEM images was not possible. The BET surface areas decreased with the temperature from 228 $m^2 g^{-1}$ for T225 dried at 160 °C under vacuum, to 220 $m^2 g^{-1}$ for T225–300, to 200

$m^2 g^{-1}$ for T225–350 and to 140 $m^2 g^{-1}$ for T225–400 (see Table 3), thus similarly corroborating the findings from PXRD and TEM.

Thermal analysis

An example of results from a TG/DTA measurement on the T225 sample is shown in Fig. 5. An exothermic peak and a corresponding substantial mass loss of *ca.* 30% were observed in the range of 300–500 °C. This behavior was typical for all samples (see ESI†). The reaction and mass loss could be ascribed to the oxidation of the remaining organic residues from the synthesis. The total mass loss of all samples (which increased further

Table 2 Crystallographic information extracted from the Rietveld refinements

| Sample	T225–300	T225–350	T225–375	T225–400	T225-375NaOH	T225-400NaOH	T225-600NaOH
Anatase weight fraction (%)	13.7(3)	30.7(3)	60.0(2)	89.1(2)	4.6(2)	7.1(1)	25.2(4)
Anatase							
Anatase size a (nm)	6.2	4.6	6.4	6.2	7.6	9.2	19.3
Anatase size c (nm)	2.4	2.7	5.2	4.9	6.4	8.9	20.0
Lattice a (Å)	3.817(1)	3.7997(5)	3.7890(1)	3.7893(1)	3.827(2)	3.810(1)	3.7835(4)
Lattice c (Å)	9.433(4)	9.505(1)	9.5070(4)	9.5070(4)	9.576(5)	9.535(3)	9.495(1)
R_f	0.473	0.616	0.783	0.676	2.72	3.68	7.82
R_{Bragg}	1.12	0.892	1.10	1.02	3.25	4.60	9.88
$TiO_2(B)$							
$TiO_2(B)$ size a (nm)	1.0	1.2	2.5	2.3	0.9	1.2	4.6
$TiO_2(B)$ size b (nm)	4.3	4.0	6.0	6.5	3.8	4.6	9.6
$TiO_2(B)$ size c (nm)	1.3	1.5	2.0	2.6	1.2	1.6	5.5
Lattice a (Å)	12.312(8)	12.249(5)	12.186(3)	12.175(2)	12.37(1)	12.32(1)	12.224(3)
Lattice b (Å)	3.7619(7)	3.7591(4)	3.7553(3)	3.7554(3)	3.779(1)	3.7741(8)	3.8209(5)
Lattice c (Å)	6.673(3)	6.625(2)	6.610(1)	6.606(1)	6.629(4)	6.599(3)	6.442(1)
Beta (degrees)	109.22(5)	109.14(4)	109.36(3)	109.31(3)	109.20(6)	108.96(6)	107.34(3)
R_f	0.556	0.532	0.553	0.569	1.02	1.53	7.79
R_{Bragg}	1.11	0.992	0.948	1.04	1.89	3.03	14.2
χ^2	4.17	4.24	3.40	5.00	8.78	12.7	19.9
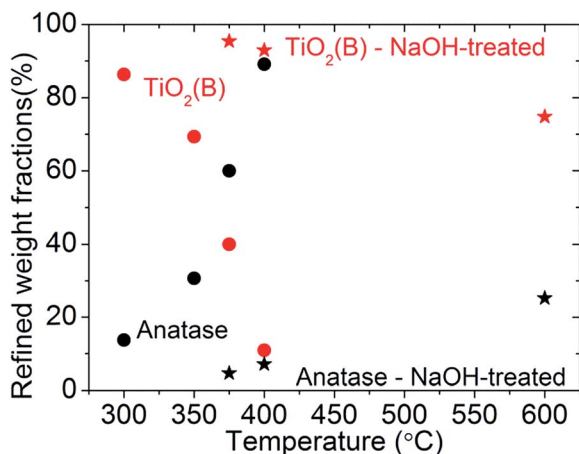
Fig. 3 The refined weight fraction of TiO$_2$(B) (red symbols) and anatase (black symbols) as a function of calcination temperature and without the addition of NaOH (circles) and with the addition of NaOH (stars).

upon cooling – indicating that no steady state was reached) can be seen in Table 1 and varied between 35 and 40%. Washing of a given sample several times with water and ethanol prior to heating only lowered the mass loss to *ca.* 30%.

In situ PXRD

In situ variable temperature PXRD of the prepared samples heated to 800 °C revealed gradual transitions of the precursors to TiO$_2$(B) and anatase nanoparticles from ~300–500 °C (see Fig. 6), in accordance with the loss of organic mass from the thermal analysis. From ~500 °C, a clear enhancement of the anatase peaks with a simultaneous diminishing of the TiO$_2$(B) peaks could be observed. Conversely, when heating the T225 sample treated with NaOH, the sample appeared to have a higher transformation temperature of the precursor at ~400 °C, where TiO$_2$(B) peaks emerged and intensified up to 800 °C with only minor traces of anatase peaks occurring. The thermal stability of the TiO$_2$(B) phase up to at least 600 °C has previously been reported by other groups.[31,32] Due to the fact that the

Table 3 BET surface areas of heated T225 samples

Sample	T225–160	T225–300	T225–350	T225–400
Surface area m^2 g^{-1}	228(5)	220(5)	200(5)	140(5)

samples lost more than one third of their mass from ~300 °C, they also shrank significantly and moved partly out of the beam, resulting in lowering of the overall intensities, and thus also the scale factor, in the recorded PXRD patterns. A further drop in intensities of the peaks was observed around 300 °C, where the TiO$_2$(B) and anatase started to grow, which coincided with the largest mass loss according to the TGA measurements. This could suggest that the organic compounds were not only present as amorphous materials surrounding the crystalline precursor material (supposedly a layered titanate) but may have been an integral part of the crystal structure. The fact that the organic contents could not easily be separated from the titania by washing with water and ethanol supported this hypothesis. The *in situ* PXRD data were in good agreement with the *ex situ* PXRD data of the samples heated in air for two hours at various temperatures (*cf.* Fig. 2). However, the NaOH treated T225 sample turned black after the heat treatment in the *in situ* setup (see ESI†). This observation could pave the way for the possibility of carbon-coating the TiO$_2$(B) particles or making hybrid-structures in oxygen-deficient atmospheres.

Electrochemical properties

In Fig. 7, examples of galvanostatic charge and discharge curves of the T225–400 and T225-400NaOH samples are shown for Li ion half cells. The T225–400 sample reached a discharge capacity of 308 mA h g^{-1}, and a charge capacity of 257 mA h g^{-1}. A first cycle capacity loss is commonly observed for TiO$_2$ especially due to surface OH- and H$_2$O-groups.[33,34] In an attempt to mitigate the first cycle irreversible capacity, based on recent work,[11] NaOH was added to the autoclaved precursor before calcination in air. While the NaOH did lower the irreversible capacity, it also altered the structural properties significantly as mentioned in the section on the structural results and hence a
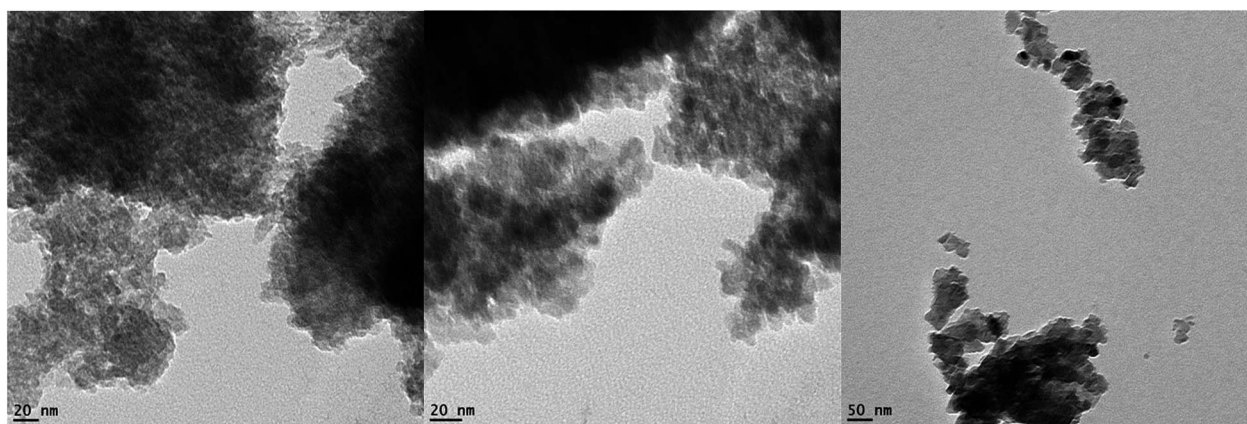

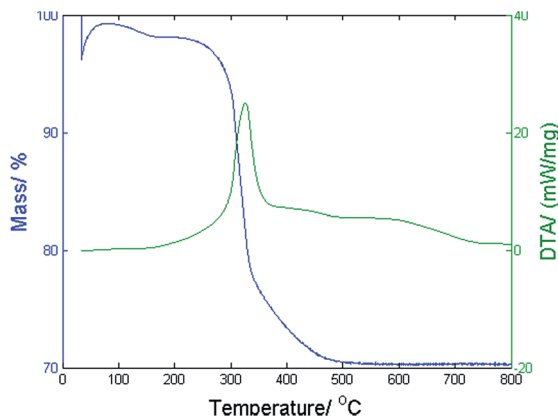Fig. 4 TEM images of left: T225, middle: T225–400 and right: T225-600NaOH. Note the different scale.

This journal is © The Royal Society of Chemistry 2015

J. Mater. Chem. A, 2015, **3**, 18667–18674 | **18671**

Fig. 5 TG/DTA graph/plot of the T225 sample heated under an Ar/O$_2$ flow.

Fig. 7 Galvanostatic charge and discharge of T225−400 (black and grey) and T225-400NaOH (blue and cyan).

direct comparison of irreversible capacity was not possible. The initial discharge capacity of T225-400NaOH reached 210 mA h g^{-1} and the charge capacity was 190 mA h g^{-1}. The lower capacities of the NaOH-treated samples appeared to be due to the lack of anatase in these samples, which was evident in the differential capacities depicted in Fig. 8. The characteristic anatase peak in the differential capacities was observed at 1.7 V *vs.* Li/Li$^+$ (discharge) and 2.0 V (charge) and the two TiO$_2$(B) peaks at 1.5/1.6 V (discharge) and 1.6/1.7 V (charge). The differential capacities concurred with the Rietveld refinement results, which showed an increasing amount of the anatase phase with increasing calcination temperature. However, the

TiO$_2$(B) phase remained unchanged in the temperature range of 350–400 °C (*cf.* TiO$_2$(B)-peaks in Fig. 8 and *in situ* PXRD Fig. 6), which indicated that the anatase phase was initially emerging and growing from the amorphous precursor at ∼300 °C, while the TiO$_2$(B) phase started transforming to anatase from ∼500°C. The charge and discharge capacities of Li-ion coin cells at various currents for the T225-samples heated at different temperatures with and without NaOH addition are plotted in Fig. 9. Noticeably, the capacities increased with calcination
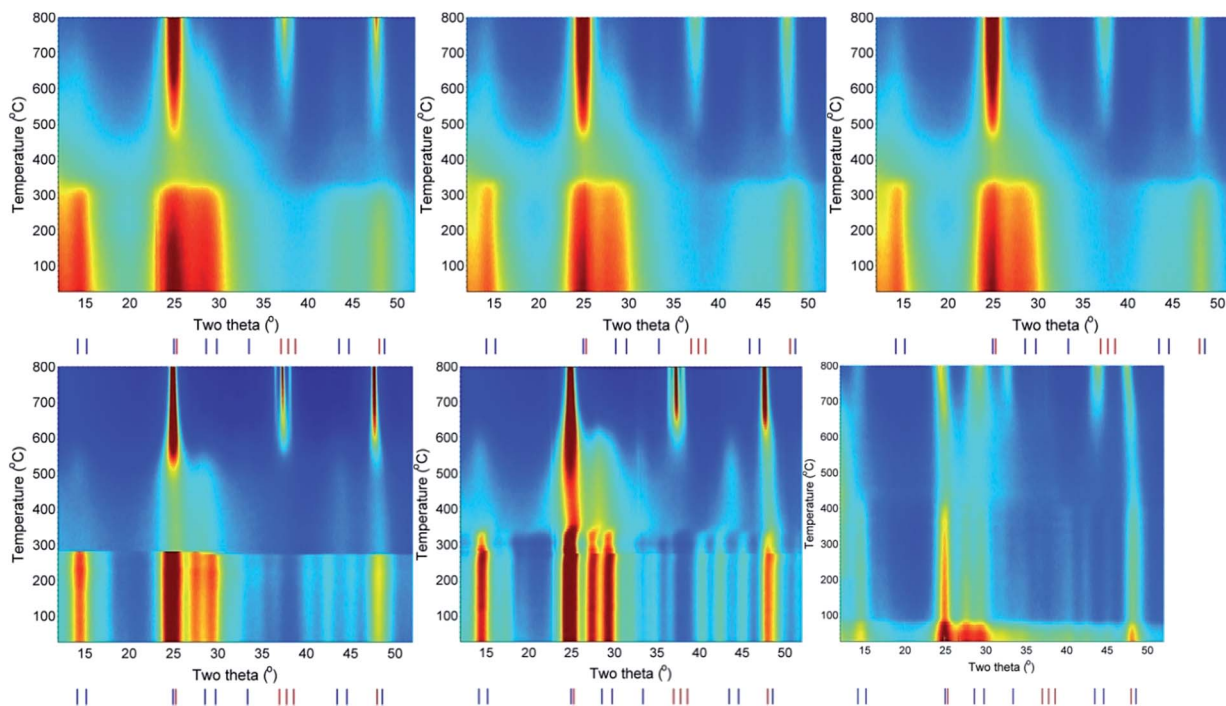

Fig. 6 *In situ* diffraction data obtained while heating the as-prepared samples from room temperature to 800 °C, upper left: T125, upper middle: T150, upper right: T175, lower left: T200, lower middle: T225 and lower right: T225-NaOH. The red and blue lines beneath each plot refer to the positions of the most intense peaks expected from anatase and bronze, respectively.
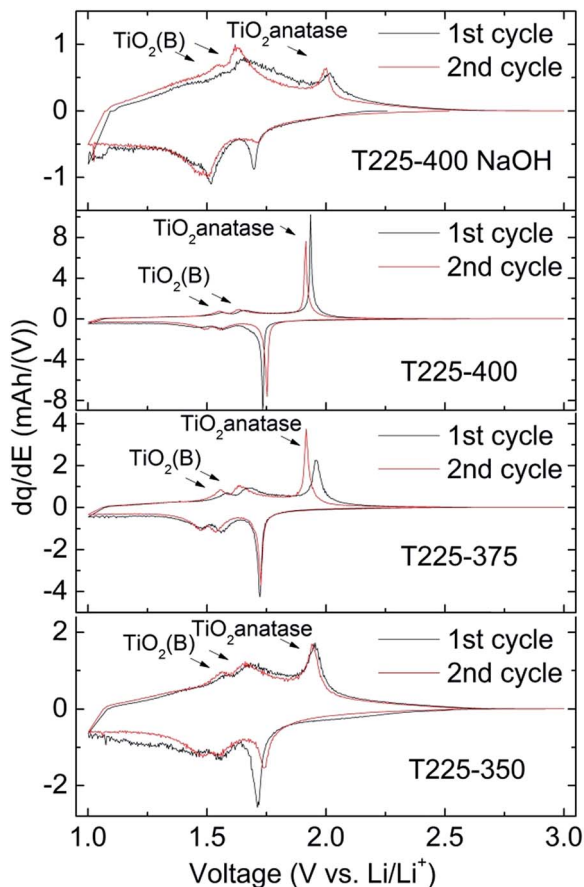
Fig. 8 Differential capacities of the first two galvanostatic cycles of four different samples from the top down: T225-400NaOH, T225–400, T225–375 and T225–350.

temperature from *ca.* 150 mA h g^{-1} for T225–300 to ∼220 mA h g^{-1} for T225–375 and T225–400 at 335 mA g^{-1}. The lower values of the T225–300 sample were partly due to the relatively large remains of the organic material. The obtained capacities
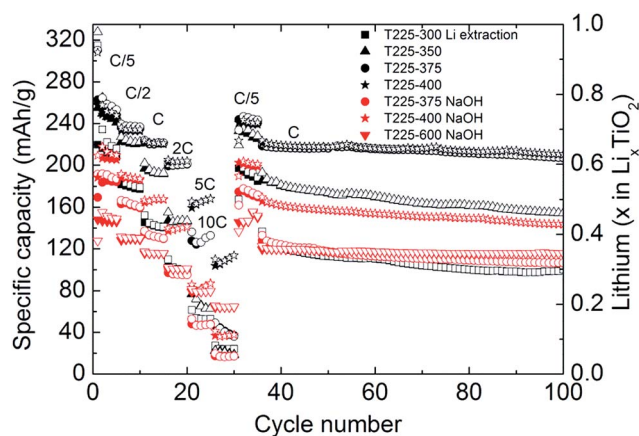

Fig. 9 Charge (filled symbols) and discharge (hollow symbols) capacities between 1 and 3 V *vs.* Li/Li$^+$ at various currents (1C = 335 mA g^{-1}) of T225-series heated at different temperatures with (red symbols) and without (black symbols) NaOH addition.
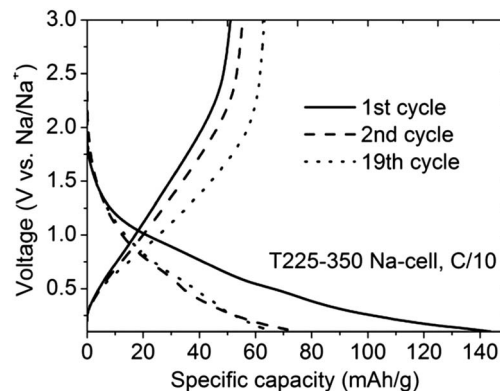

Fig. 10 Voltage *vs.* specific capacity at 33.5 mA g^{-1} between 0.1 and 3.0 V of sample T225−350 in a Na-half cell.

in the T225–400 sample were comparable with the best previously reported TiO$_2$ capacities (see ref. 11 and 35 and references therein). The rate-performance was additionally enhanced as a function of the calcination temperature and the T225–400 retained a capacity of ∼110 mA h g^{-1} at 3350 mA g^{-1}. The NaOH-treated samples exhibited lower capacities compared with the non-treated ones that were calcined at the same temperatures. Although a higher ratio of TiO$_2$(B) to anatase could be expected to yield improved electrochemical performance, the decreased capacities of the NaOH-treated samples may be due to the formation of an inactive Na-titanate layer or unreacted NaOH on the surface of the TiO$_2$ particles. It is well known that alkali-titanates can be formed from solid state reactions of TiO$_2$ with alkali-hydroxides. The further decrease of performance of the T225-600NaOH sample could be due to the increase in the Na-titanate layer as well as the increase in size as observed in the refinements of PXRD data and TEM images.

The charge and discharge capacities of the T225–350 sample in Na-half cells can be seen in Fig. 10 and 11. An initial discharge capacity of 140 mA h g^{-1} was observed, however, upon subsequent cycling the reversible capacity was only *ca.* 60 mA h g^{-1}. This was significantly lower than those in recent reports of promising electrochemical performance of TiO$_2$ in Na-ion half-cells, where reversible capacities of typically 150 mA h g^{-1} were achieved.[5–10]
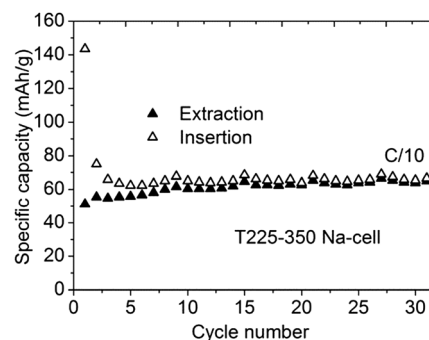

Fig. 11 Cycle-test of T225−350 in a Na-half cell charged to 3.0 V and discharged to 0.1 V at 33.5 mA g^{-1}.

4. Conclusions

The synthesis of $TiO_2(B)$/anatase mixtures by a facile route has been investigated in detail by applying various precursor concentrations and temperatures. The evolution of the $TiO_2(B)$ and anatase phases were monitored employing *ex* and *in situ* powder X-ray diffraction combined with Rietveld refinement. It was found that from *ca.* 375 °C, anatase became the dominating phase, however, the addition of NaOH before calcination could mitigate the anatase formation and retain $TiO_2(B)$ as the main phase up to at least 800 °C. Furthermore, the electrochemical performance in Li- and Na-ion coin cells was evaluated and a performance comparable to the best previously reported results of TiO_2 in Li-cells was achieved. The results from the Na-cells were less encouraging.

Acknowledgements

Notes and references

1 P. Roy, S. Berger and P. Schmuki, *Angew. Chem., Int. Ed.*, 2011, **50**, 2904–2939.

2 T. Froschl, U. Hormann, P. Kubiak, G. Kucerova, M. Pfanzelt, C. K. Weiss, R. J. Behm, N. Husing, U. Kaiser, K. Landfester and M. Wohlfahrt-Mehrens, *Chem. Soc. Rev.*, 2012, **41**, 5313–5360.

3 C. Jiang and J. Zhang, *J. Mater. Sci. Technol.*, 2013, **29**, 97–122.

4 X. Su, Q. Wu, X. Zhan, J. Wu, S. Wei and Z. Guo, *J. Mater. Sci.*, 2012, **47**, 2519–2534.

5 Y. Xu, E. M. Lotfabad, H. Wang, B. Farbod, Z. Xu, A. Kohandehghan and D. Mitlin, *Chem. Commun.*, 2013, **49**, 8973–8975.

6 H. A. Cha, H. M. Jeong and J. K. Kang, *J. Mater. Chem. A*, 2014, **2**, 5182–5186.

7 L. Wu, D. Buchholz, D. Bresser, L. Gomes Chagas and S. Passerini, *J. Power Sources*, 2014, **251**, 379–385.

8 J. P. Huang, D. D. Yuan, H. Z. Zhang, Y. L. Cao, G. R. Li, H. X. Yang and X. P. Gao, *RSC Adv.*, 2013, **3**, 12593–12597.

9 S.-M. Oh, J.-Y. Hwang, C. S. Yoon, J. Lu, K. Amine, I. Belharouak and Y.-K. Sun, *ACS Appl. Mater. Interfaces*, 2014, **6**, 11295–11301.

10 Z. Yan, L. Liu, J. Tan, Q. Zhou, Z. Huang, D. Xia, H. Shu, X. Yang and X. Wang, *J. Power Sources*, 2014, **269**, 37–45.

11 M. Søndergaard, Y. Shen, A. Mamakhel, M. Marinaro, M. Wohlfahrt-Mehrens, K. Wonsyld, S. Dahl and B. B. Iversen, *Chem. Mater.*, 2014, **27**, 119–126.

12 S. Liu, H. Jia, L. Han, J. Wang, P. Gao, D. Xu, J. Yang and S. Che, *Adv. Mater.*, 2012, **24**, 3201–3204.

13 H. Liu, Z. Bi, X.-G. Sun, R. R. Unocic, M. P. Paranthaman, S. Dai and G. M. Brown, *Adv. Mater.*, 2011, **23**, 3450–3454.

14 J. Wang, Y. Zhou and Z. Shao, *Electrochim. Acta*, 2013, **97**, 386–392.

15 Y. Tang, Y. Zhang, J. Deng, J. Wei, H. L. Tam, B. K. Chandran, Z. Dong, Z. Chen and X. Chen, *Adv. Mater.*, 2014, **26**, 6111–6118.

16 R. Marchand, L. Brohan and M. Tournoux, *Mater. Res. Bull.*, 1980, **15**, 1129–1133.

17 C. Wessel, L. Zhao, S. Urban, R. Ostermann, I. Djerdj, B. M. Smarsly, L. Chen, Y.-S. Hu and S. Sallard, *Chem.–Eur. J.*, 2011, **17**, 775–779.

18 G. Xiang, T. Li, J. Zhuang and X. Wang, *Chem. Commun.*, 2010, **46**, 6801–6803.

19 M. Kobayashi, V. V. Petrykin, M. Kakihana, K. Tomita and M. Yoshimura, *Chem. Mater.*, 2007, **19**, 5373–5376.

20 A. R. Armstrong, G. Armstrong, J. Canales, R. García and P. G. Bruce, *Adv. Mater.*, 2005, **17**, 862–865.

21 S. Brutti, V. Gentili, H. Menard, B. Scrosati and P. G. Bruce, *Adv. Energy Mater.*, 2012, **2**, 322–327.

22 Z. Zhang, Z. Zhou, S. Nie, H. Wang, H. Peng, G. Li and K. Chen, *J. Power Sources*, 2014, **267**, 388–393.

23 J. Rodriguezcarvajal, *Phys. B*, 1993, **192**, 55–69.

24 N. Lock, P. Hald, M. Christensen, H. Birkedal and B. B. Iversen, *J. Appl. Crystallogr.*, 2010, **43**, 858–866.

25 M. Jarvinen, *J. Appl. Crystallogr.*, 1993, **26**, 525–531.

26 N. C. Popa, *J. Appl. Crystallogr.*, 1998, **31**, 176–180.

27 C. Tyrsted, K. M. O. Jensen, E. D. Bojesen, N. Lock, M. Christensen, S. J. L. Billinge and B. B. Iversen, *Angew. Chem., Int. Ed.*, 2012, **51**, 9030–9033.

28 J. R. Eltzholtz, C. Tyrsted, K. M. O. Jensen, M. Bremholm, M. Christensen, J. Becker-Christensen and B. B. Iversen, *Nanoscale*, 2013, **5**, 2372–2378.

29 G. Li, L. Li, J. Boerio-Goates and B. F. Woodfield, *J. Am. Chem. Soc.*, 2005, **127**, 8659–8666.

30 I. E. Grey and N. C. Wilson, *J. Solid State Chem.*, 2007, **180**, 670–678.

31 W. Zhou, L. Gai, P. Hu, J. Cui, X. Liu, D. Wang, G. Li, H. Jiang, D. Liu, H. Liu and J. Wang, *CrystEngComm*, 2011, **13**, 6643–6649.

32 W. Zhuang, L. Lu, X. Wu, W. Jin, M. Meng, Y. Zhu and X. Lu, *Electrochem. Commun.*, 2013, **27**, 124–127.

33 W. J. H. Borghols, D. Luetzenkirchen-Hecht, U. Haake, W. Chan, U. Lafont, E. M. Kelder, E. R. H. van Eck, A. P. M. Kentgens, F. M. Mulder and M. Wagemaker, *J. Electrochem. Soc.*, 2010, **157**, A582–A588.

34 M. Wagemaker and F. M. Mulder, *Acc. Chem. Res.*, 2012, **46**, 1206–1215.

35 J. Qu, J. E. Cloud, Y. Yang, J. Ding and N. Yuan, *ACS Appl. Mater. Interfaces*, 2014, **6**, 22199–22208.

18674 | *J. Mater. Chem. A*, 2015, **3**, 18667–18674

This journal is © The Royal Society of Chemistry 2015